Engineering P450 TamI as an iterative biocatalyst for selective late-stage C-H functionalization and epoxidation of tirandamycin antibiotics

Rosa V. Espinoza,[1,2] Kersti Caddell Haatveit,[6] S. Wald Grossman,[1] Jin Yi Tan,[1] Caylie A. McGlade,[1] Yogan Khatri,[1] Sean A. Newmister,[1] Jennifer J. Schmidt,[1] Marc Garcia-Borràs,[6] John Montgomery,[4] K. N. Houk,[6] David H. Sherman[1,3,4,5*]

[1]Life Sciences Institute, [2] Program in Chemical Biology, [3]Department of Medicinal Chemistry, [4]Department of Chemistry, [5]Department of Microbiology and Immunology, University of Michigan, Ann Arbor, Michigan 48109, United States
[6]Department of Chemistry and Biochemistry, University of California, Los Angeles, California 90095, United States

Abstract

Iterative P450 enzymes are powerful biocatalysts for selective late-stage C-H oxidation of complex natural product scaffolds. These enzymes represent new tools for selectivity and cascade reactions, facilitating direct access to core structure diversification. Recently, we reported the structure of the multifunctional bacterial P450 TamI and elucidated the molecular basis of its substrate binding and strict reaction sequence at distinct carbon atoms of the substrate. Here, we report the design and characterization of a *toolbox* of TamI biocatalysts, generated by mutations at Leu101, Leu244 and/or Leu295, that alter the native selectivity, step sequence and number of reactions catalyzed, including the engineering of a variant capable of catalyzing a four-step oxidative cascade without the assistance of the flavoprotein and oxidative partner TamL. The tuned enzymes override inherent substrate reactivity enabling catalyst-controlled C-H functionalization and alkene epoxidation of the tetramic acid-containing natural product tirandamycin. Five new, bioactive tirandamycin derivatives (6-10) were generated through TamI-mediated enzymatic synthesis. Quantum mechanics calculations and MD simulations provide important insights on the basis of altered selectivity and underlying biocatalytic mechanisms for enhanced continuous oxidation of the iterative P450 TamI.

Introduction

Ubiquitous in all domains of life, cytochrome P450 enzymes represent a versatile platform for the controlled functionalization of specific, nonactivated C-H bonds within complex organic molecules.[1, 2] These heme-containing biocatalysts introduce late-stage functionality with precise regio-, chemo- and stereoselectivity, expanding the synthetic abilities of chemical oxidation catalysts and reagents for structural diversification of biologically important molecules.[3, 4] In rare cases for select secondary metabolite pathways, the iterative control of C-H oxidation and epoxidation is observed, typically in plant or fungal systems.[5-8] Understanding the function of iterative P450s is a first step toward gaining the ability to tune these multi-step biocatalytic oxidations through protein engineering, a challenging goal for development of efficient oxidative tailoring strategies.[9, 10]

Eukaryotic iterative P450s are often bound to the endoplasmic reticulum membrane, and frequently challenging to express as recombinant proteins *in vitro*, which has limited our mechanistic understanding of their reactivity and selectivity.[5] Investigating their soluble bacterial counterparts can address this gap in knowledge and lead to the development of biocatalysts with high synthetic utility. Currently, the number of characterized iterative bacterial P450s is scarce, and most are restricted to catalyzing two oxidation events. Examples include P450s MycG[11, 12] and Gfsf,[13] in the biosynthesis of the macrolide antibiotics mycinamicin and FD-891, respectively, and the P450 AurH,[14] involved in the biosynthesis of the nitroaryl-substituted polyketide aureothin. The cytochrome P450 TamI, from the tirandamycin biosynthetic system, represents a rare example of a bacterial P450 naturally catalyzing three highly selective, successive oxidation reactions at distinct carbon atoms of the substrate (Figure 1).[15, 16]

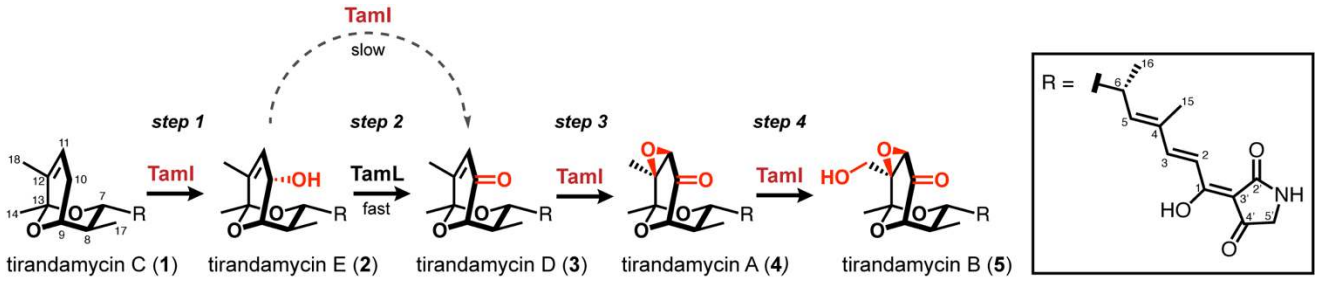

Figure 1. Iterative late-stage oxidation reactions catalyzed by the P450 TamI. In *step 1*, TamI catalyzes an allylic hydroxylation at C10 of **1**. In *step 2*, the flavoprotein TamL oxidizes the C10 hydroxyl of **2** to a ketone. In *step 3*, TamI performs an alkene epoxidation at C11/12 of **3.** In *step 4*, TamI installs a primary hydroxyl at C18 of **4** yielding the terminal product **5**.

Tirandamycin comprises a small family of structurally intriguing dienoyltetramic acid-containing natural products formed through a hybrid polyketide synthase (PKS) and non-ribosomal peptide synthetase (NRPS) system.[17] Originally discovered in 1971,[18] a total of 15 tirandamycin congeners have been reported from various bacterial species including the marine-derived *Streptomyces* sp. 307-9 (Figure S1). We previously characterized new intermediates tirandamycin C **(1)**, E **(2)** and D **(3)**, in a search for lead molecules against the vancomycin resistant *Enterococcus faecalis* (VRE) and determined that the heavily oxygenated bicyclic ketal moiety of tirandamycin is key to bioactivity.[15, 19] Other biological properties reported for tirandamycin metabolites include potent *in vitro* activity against lymphatic filariasis-causing *Brugia malayi* adult parasites,[20] inhibition of the futalosine pathway (an operative pathway in *Helicobacter pylori*)[21] and specific anticancer effects in a *Drosophila* tumor model by inhibition of asparaginyl-tRNA synthetase.[22]

Two tailoring enzymes are responsible for the sequential late-stage installation of the oxygen functionalities during tirandamycin biosynthesis: the P450 TamI and the flavin oxidase TamL (Figure 1).[15] First, TamI abstracts the C10-(*S*) hydrogen of **1** to install an allylic hydroxyl (*step 1*) generating **2**, which undergoes oxidation by TamL (*step 2*) to yield **3**. Next, TamI catalyzes the formation of a C11/C12 (*R*/*S*) epoxide (*step 3*) producing **4**, followed by methyl hydroxylation at C18 (*step 4*) generating the terminal product **5**. TamI has been shown to oxidize **1** → **2** → **3** → **4** at low levels without the need for TamL,[15] suggesting the possibility of a more complex iterative

mechanism in some instances. Based on gene deletion studies and isolation of biosynthetic intermediates, the unusual iterative cascade catalyzed by TamI occurs in a strict sequence, with each oxidation being a prerequisite for the next.[15, 17]

The promising biological activities and molecular complexity of tirandamycins has attracted considerable attention from synthetic chemists for the last 40 years.[23-25] Although notable routes have been developed for the racemic and enantioselective construction of this synthetic target, they rely on extensive functional group manipulation for introducing the oxygen atoms decorating the bicyclic moiety. Synthetic approaches often are designed for a specific member of this natural product group, with the oxidation level pre-defined at an early stage of the synthesis. Developing an approach that employs late-stage oxidations enabled by biocatalyst modification would facilitate efficient diversification of tirandamycin molecules for further optimization of pharmacological properties. Based on our previous work, we envisioned that structure-based engineering of the trifunctional P450 TamI could provide important new insights into the controlling elements of its oxidative cascade, allowing us to manipulate the enzyme to develop new tools for catalyst-controlled iterative C-H oxidation and epoxidation with altered selectivity and step sequence.

Herein, we report the design and characterization of a *toolbox* of P450 TamI biocatalysts, generated by point mutations, that control the sequence and site-selectivity of epoxidation and C-H oxidation of tirandamycin molecules, achieving divergent reactivity compared to wild-type (WT) enzyme. Using these tuned catalysts, a series of novel tirandamycin derivatives were generated from a single molecular scaffold and evaluated for activity against a panel of human bacterial pathogens. Utilizing active-site engineering, a TamI variant with remarkably enhanced catalytic abilities was developed, overriding the need for the oxidative partner TamL, and enabling a direct four-step biocatalytic cascade for the construction of **5** from **1**. Furthermore, quantum mechanics (QM) and molecular dynamics (MD) simulations were conducted to examine the basis for TamI mutant selectivity and provided new insights into reaction mechanisms of this catalyst-controlled system.

Results

We recently reported the structure of TamI in complex with **1** and found that active-site hydrophobic residues have a significant influence in substrate binding and step sequence reactivity, favoring C10 C-H hydroxylation (Figure 1, *step 1*) as the first catalytic reaction.[16] Computational experiments suggested that TamI's unique active site geometry is key to discriminating between the diastereomeric transition states leading to **2**. However, preliminary mutagenesis efforts failed to reveal how TamI modulates substrate orientation to favor the (*S*) enantiomer, or how the enzyme controls the strict sequence of oxidation. Thus, the specific molecular factors controlling this selectivity and order of steps remained elusive despite a high-resolution x-ray structure of the substrate-TamI complex.

We envisioned identifying key active site residues that dictate the selectivity and step sequence displayed by TamI. Thus, amino acids within 5Å of the tirandamycin bicycle were

selected for an alanine/valine scan by single point mutation (Figure 2), generating a total of 13 TamI mutants: L101A, L101V, L244A, L244V, L295A, L295V, I247A, I247V, G248A, T251A, T299A, T299V and H102V (Figure 3). Enzymatic conversions of **1** were conducted *in vitro* using a previously optimized three-component system comprising spinach ferredoxin, ferredoxin reductase and P450 TamI in the presence of a NADPH cofactor regeneration system. Initial analytical evaluation of the 13 mutants revealed nearly WT activity for all but five specific positions, revealing potential key residues in both the binding and positioning of the tirandamycin substrate. Of the five, the TamI H102V variant resulted in severe loss of catalytic activity highlighting its likely role in substrate binding as previously described,[16] through a proposed interaction between the Nε of His102 and the oxygen atoms of the ketal group (Figure 3A, lane 11).

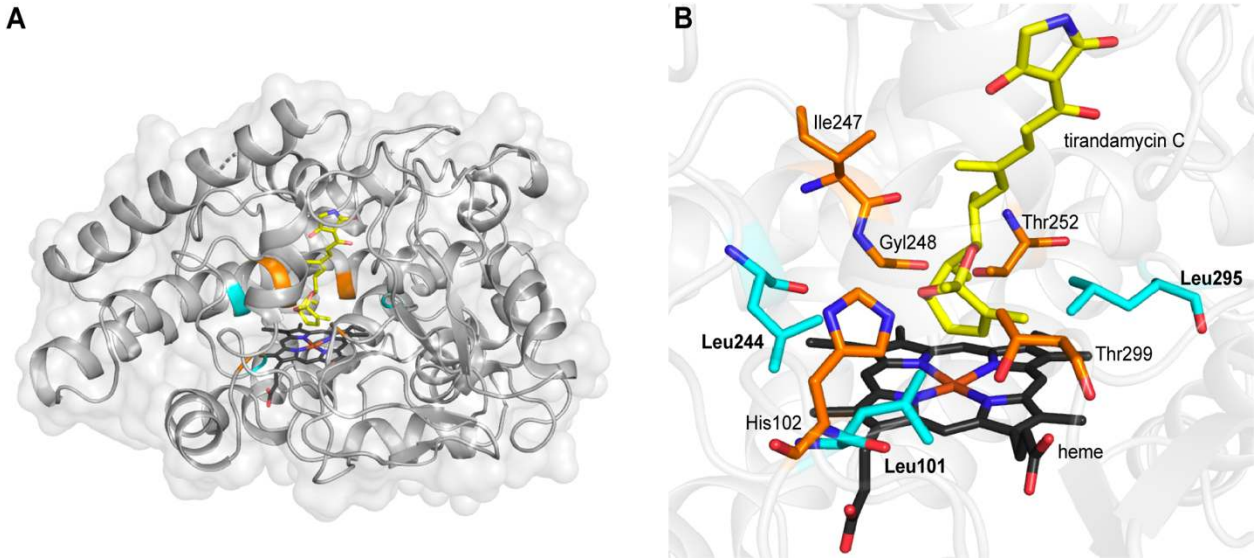

Figure 2. Active-site residues of TamI located within 5Å of the tirandamycin bicycle and selected for an alanine-valine scan. (A) Cartoon representation of TamI in complex with **1** (shown in yellow). The three amino acids found to be critical in controlling TamI's selectivity and iterative oxidation are highlighted in cyan; the remaining amino acids mutated are shown in orange. (B) Stick representation.

1.1 Identification and engineering of TamI mutants with divergent selectivity from WT

Analysis of products formed from the TamI L244A mutant revealed trace amounts of a new double oxidation congener (**11**) (Figure 3A, lane 8). The selectivity of L101A was poor, producing a mixture of an unknown single oxidation intermediate (**6**), and two new double oxidation congeners with variant polarities (**7** and **8**) (Figure 3A, lane 7). The alanine substitution may hamper the ability of the substrate to adopt one distinct orientation within the enzyme binding pocket, leading to multiple oxidation products. On the other hand, this catalytic flexibility makes L101A a promising starting point toward engineering selective TamI variants for the production of each of these new congeners. TamI L295V led to the preferential formation of **7**, the least polar double oxidation congener indicated above (Figure 3A, lane 10), while TamI L295A selectively produced two unique triple oxidation products that eluted as a single peak (**9** and **10**)

(Figure 3A, lane 9). This divergent reactivity suggests that subtle steric factors at the Leu295 position significantly alter the substrate binding orientation with respect to the heme center.

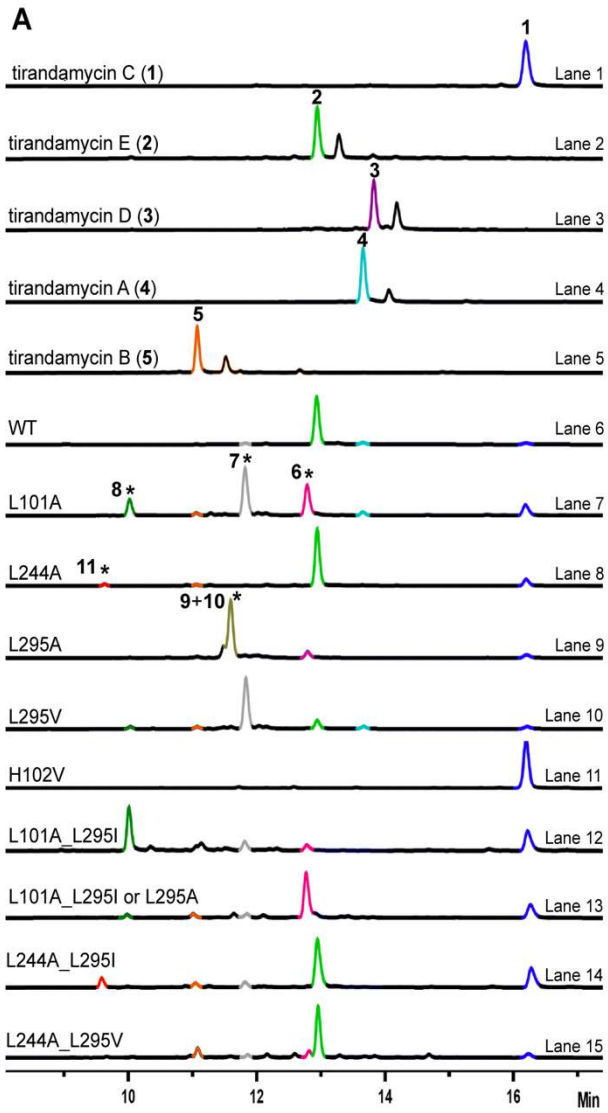

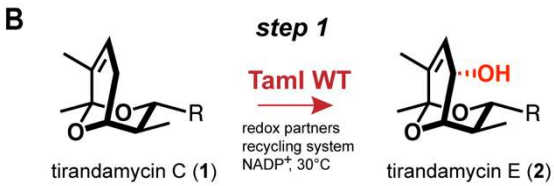

P450 TamI	Main product(s)	Step(s) catalyzed	Lane
WT	**2**	1	6
L101V, L244V, I247V, G248A, T252A, T299A, T299V	**2**	1	see SI
L295A	*9 + *10 (11.6 min) New triple ox.	3 + additional new steps	9
L295V	*7 (11.8 min) New double ox.	1 + 3	10
H102V	no conversion	none	11
L101A_L295I	*8 (10 min) New double ox.	3 + 4	12
L101A_L295I or L295A (reaction conditions adjusted)	*6 (12.7 min) New single ox.	3	13
L244A_L295I	**2** + *11 (9.6 min) New double ox.	1	14
L244A_L295V	**2 + 5**	1 + 2 + 3 + 4	15

Figure 3. Endpoint assays with TamI mutants. (A) LC-MS traces (extracted at 354nm, signature UV of tirandamycin) of select reactions (refer to Figure S2 for additional LC-MS traces). Authentic standards include **1-5** (lanes 1-5). Compounds **2-5** show a sister peak due to isomerization in methanol. Peaks of new tirandamycin congeners are marked with an asterisk (lanes 7-9). All reactions were performed following standard conditions (see Methods) except for lane 13 reaction that included 1µM P450 L101A_L295I catalyst loading instead of 2µM. The new single oxidation congener (12.7 min) was also generated as the major product with P450 L295A as the catalyst when adjusting reaction parameters. (B) Summary of *in vitro* analytical enzymatic reactions with TamI variants and **1**. The steps catalyzed by each mutant are shown in sequential order of reactivity where *step 1* is C10 hydroxylation, *step 2* is C10 ketone formation, *step 3* is C11/12 epoxidation and *step 4* is C18 hydroxylation as shown in Figure 1.

TamI mutants displaying non-selective product profiles (TamI L101A and TamI L244A) were further engineered to improve selectivity and maximize production of the new

tirandamycin congeners. The double variant L101A_L295V favored production of **8** that single mutants L101A and L295V generated in small amounts. Although increased formation of the desired product was observed, this double variant expressed poorly in *E. coli*. We addressed this complication by introducing L295I instead, which was one of the highest producing single mutant forms of TamI. Thus, TamI L101A_L295I selectively produced **8** as the major product (Figure 3A, lane 12). Following a similar strategy, the L244A_L295I double mutant was generated in an effort to improve formation of **11**. This double mutant catalyzed increased conversion of **1** to the desired product (Figure 3A, lane 14) compared to single variant L244A, albeit in poor yield. Moreover, adjusting reaction parameters (enzyme concentration and time) with mutants L101A_L295I and L295A favored accumulation of the single oxidation product **6** (Figure 3A, lane 13), suggesting it may be an intermediate to the more highly oxidized derivatives.

The best performing TamI mutants with divergent selectivity from WT (L295A, L295V, L101A_L295I and L244A_L295I) were chosen for further experimental work. This included biochemical characterization and large-scale enzymatic reactions to generate sufficient amounts of the new tirandamycins for structure elucidation and mechanistic studies.

1.2 Engineering of a TamI mutant with enhanced iterative capabilities

Our earlier work demonstrated that the flavin oxidase TamL serves as a co-dependent participant in conversion of **2** to **3** (Figure 1, *step 2*).[15] We envisioned engineering a TamI biocatalyst capable of more complete oxidation, forming **5** from **1** in a 4-step cascade approach in the absence of TamL. LC-MS analysis revealed that mutants L101A, L244A and L295V formed **5** in trace amounts (Figure 3A, lanes 7, 8 and 10). Notably, P450 L244A_L295V converted **1** to **5** in larger amounts than the corresponding single mutant forms (Figure 3A, lane 15), and represents a TamI variant able to catalyze up to an eight-electron oxidation cascade. The sterically less hindered replacements may relax the conformational constraints of the substrate in the active site, favoring productive binding and orientation of the more highly oxidized tirandamycin intermediates, enabling a more continuous oxidation in the absence of the flavoprotein TamL. Based on this result, TamI L244A_L295V (also referred to as the *iterative* mutant) was selected for additional experimental studies (see below).

2 Elucidation of new tirandamycin congeners and mechanism for TamI catalysis

Optimization of fermentation conditions of a *Streptomyces* sp. 307-9 Δ*tamI* P450 mutant strain enabled reliable production of **1** in a 10-20mg/L yield. This material was employed for subsequent preparative-scale enzymatic reactions to obtain sufficient starting material for structural characterization using TamI and its variants. NMR analysis, MD simulations, QM calculations and end-point assays revealed that the engineered TamI mutants have altered the selectivity and order of steps programmed into the WT enzyme to create new compounds. These studies provide additional knowledge on the TamI mechanism of iterative oxidation and represent new tools for selectivity in C-H functionalization and alkene epoxidation.

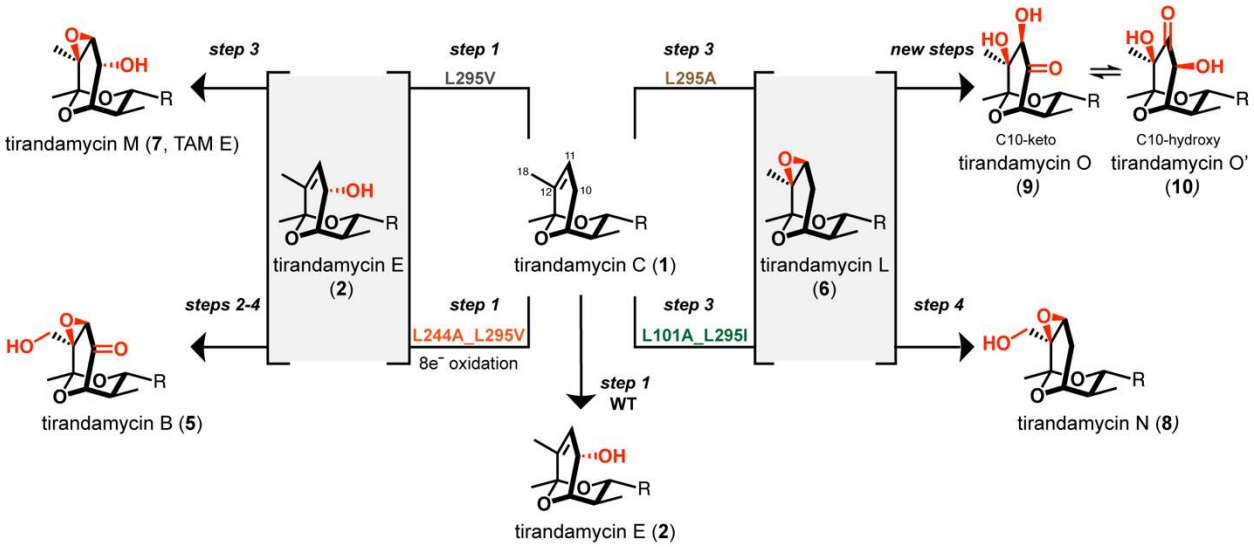

Figure 4. TamI mutants generating novel tirandamycin congeners with divergent selectivity from wild-type enzyme. TamI L244A_L295V performs a 4-step oxidation cascade. New tirandamycin biosynthesized include tirandamycin L **(6)**, M **(7)**, N **(8)**, O **(9)** and O' **(10)**. For complete NMR characterization data including NOE correlations, refer to SI. For PyMOL and MD simulations of TamI mutants, see Figures S5-S6.

2.1 TamI mutants L101A_L295I and L295A interrupt the native stepwise oxidative cascade, bypassing *step 1* and *step 2*, and directly catalyzing *step 3* to generate tirandamycin L (6).

Diverging from native reactivity where C10 allylic hydroxylation (*step 1*) is the first oxidation event to occur, TamI L101A_L295I and L295A catalyzed the C11/12 epoxidation (*step 3*) of **1** generating a new single oxidation congener tirandamycin L **(6)** (Figure 4; for LC-MS traces of the reactions described, refer to the SI). The stereochemistry of **6** was determined based on the observed NOE correlations of H-11 to H-7. The characterization of **6** indicates that the apparent strict stepwise oxidative cascade of TamI has been interrupted. Previous density functional theory (DFT) calculations comparing the transition state barriers for C10 hydroxylation, C11/12 (*R*/*S*) epoxidation and C18 hydroxylation starting from **1** revealed that the olefin epoxidation is highest in energy by 2.6 kcal/mol.[16] This suggests that subtle variations in the catalytic environment of TamI L101A_L295I and L295A are critical for catalyzing the least favored reaction, by potentially reorienting the substrate to lower the activation barrier. MD simulations of TamI L101A_L295I with **1** were analyzed and compared to those of TamI WT. These experiments revealed that L101A_L295I demonstrated two major binding poses: the first similar to the WT with the C10-(*S*) hydrogen oriented in the correct geometry for C–H abstraction reactivity and the second with the correct geometry for the olefin epoxidation to occur (Figure 5A). These two poses are highlighted in a comparison of the MD snapshots to the ideal transition state geometry from DFT. One analyzes *step 1*, which compares the O_{heme}-C10 H distance and O_{heme}–H10–C10 angle and demonstrates a newly introduced competition with the C10-(*R*) that was not observed in the WT, as more of the MD snapshots show the correct geometry for C10-(*S*) reactivity in the WT. The other analyzes *step 3*, which compares the O_{heme}–C11 distance and O_{heme}–C11–C12–C18 dihedral angle and shows the change in facial selectivity between the

binding poses. Thus, some of the snapshots are close to the ideal transition state dihedral angle and the rest are the opposite, allowing the possibility of the epoxidation to occur with the second binding pose. In addition, MD simulations of TamI L295A with **1** showed that proximity of the C11 atom to the heme center is maintained for the majority of the simulation, consistent with C11/12 epoxidation (Figure S11). These observations indicate that the hydrophobic interactions around the bicyclic ketal are most critical for redirecting oxidative pathways in TamI from an allylic C-H oxidation to an epoxidation event.

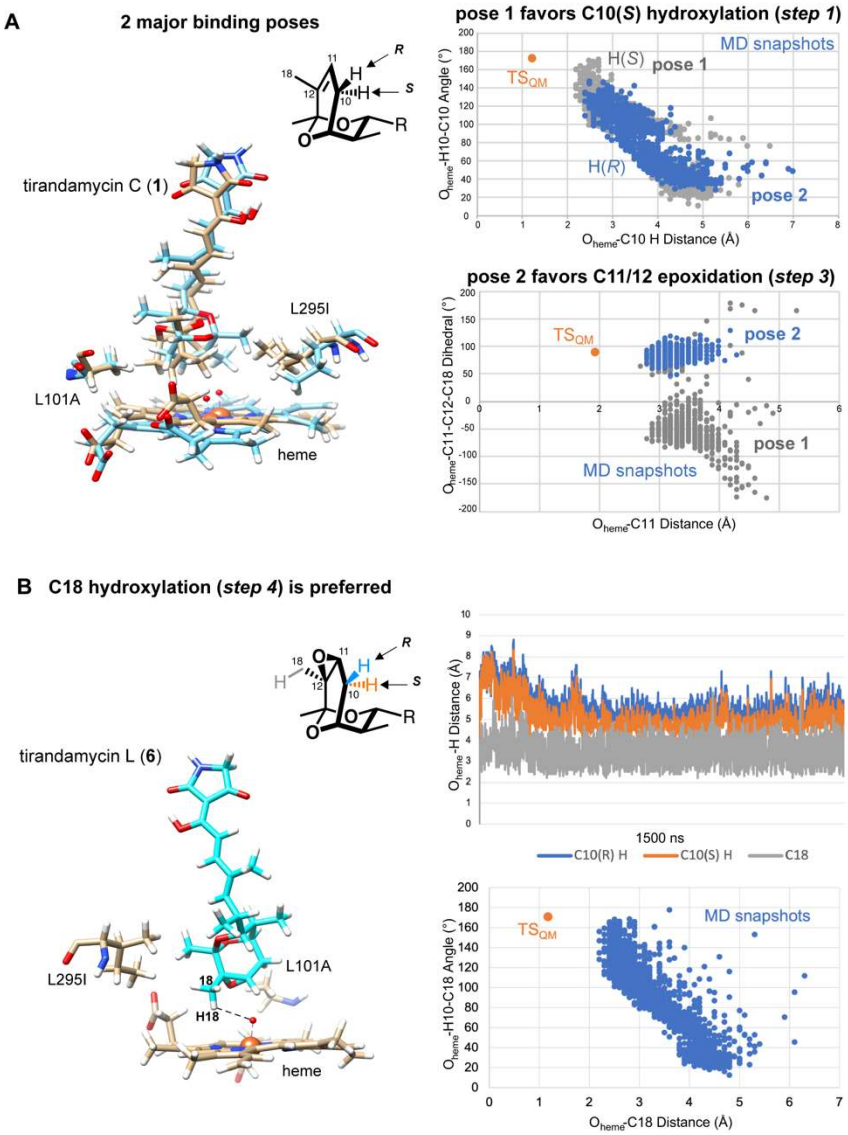

Figure 5. Computational analysis of TamI L101A_L295I. (A) MD simulations of TamI variant with **1** demonstrate two binding modes for the substrate that allow for competition for reactivity for C11/12 epoxidation (*step* 3) over C10 hydroxylation (*step 1*), as opposed to that of the WT. The second binding pose (blue) promotes a geometry that is suitable for epoxidation, supporting the experimentally observed product. (B) MD simulations with **6** shows preference for the C18 position over C10.

2.2 Dual-function TamI L295V catalyzes *step 1* and *step 3*, omitting *step 2* to generate tirandamycin M (7, also known as TAM E).[20]

Analogous to WT activity, TamI L295V first catalyzes *step 1* forming **2** from **1**. However, the next tailoring step for this variant is *step 3* on substrate **2** to generate the double oxidation congener tirandamycin M **(7**, **TAM E)** (Figure 4). Although this molecule has been previously isolated from *Streptomyces* sp. 17944,[20] our work demonstrates its production *in vitro* using a TamI P450 mutant as a biocatalyst (Table S3). MD was similarly performed with TamI L295V and **2**, which showed that a lower energy conformation was achieved after initial minimization. It also revealed that the C11 remained closest relative to other reactive positions and the oxo-iron species throughout the 1500 ns simulation, consistent with C11/12 epoxidation (Figure S11). Moreover, HPLC analysis of the culture broth of a *Streptomyces* sp. 307-9 Δ*tamL* flavoprotein mutant strain[15] revealed the presence of **2** and **7**, in approximately a 2:1 ratio, after only four days of growth (Figure S12). We reasoned that in the absence of the flavoprotein, the TamI WT is capable of catalyzing the epoxidation of **2** → **7** *in vivo*. This hypothesis is supported by the observation that when testing **2** with purified TamI WT, **7** is generated albeit as a trace product.

2.3 TamI L101A_L295I catalyzes *step 3* and *step 4*, avoiding oxidation at C10 and producing tirandamycin N (8)

After initially catalyzing the most energetically demanding reaction (*step 3*) on **1** to form intermediate **6**, TamI L101A_L295I performs *step 4* resulting in the double oxidation congener, tirandamycin N **(8)** (Figure 4). The electronegative hydroxy moiety at C18 decreases the electron density around the neighboring protons, causing less shielding and increasing the chemical shift of C18 to 58.9 ppm compared to the typical 15-16 ppm observed in tirandamycin congeners lacking this functionality.[15, 19] The disappearance of the singlet corresponding to protons of the C18 methyl group, and the presence of new signals relating to a methylene group corroborates this assignment. DFT calculations were performed to determine the transition state barrier for competing hydroxylation reactions at C18 and C10 starting from **6**. The C-H abstraction barrier for the C10(*S*) hydroxylation and C18 hydroxylation had essentially no energy difference at 0.6 kcal/mol with the former being lower in energy (Figure 6). This contradicts the experimentally observed regioselectivity with TamI L101A_L295I, where **8** is exclusively formed from **6**. MD simulations performed with the variant and **6** showed that the C18 is closest to the reactive heme iron-oxo throughout the entire 1500 ns simulation, consistent

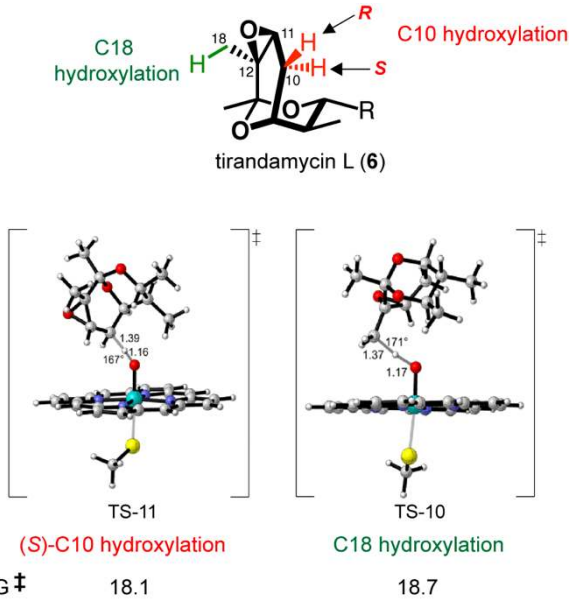

Figure 6. DFT calculations of TamI L101A_L295I regioselectivity. Intrinsic energy for the competing C-H oxidation reactions at C10 and C18 with **6** as substrate.

with *step 4* (Figure 5B). The O_{heme}-C18 hydrogen distance and O_{heme}-C18 hydrogen-C18 angle geometries from the MD simulations were compared to the ideal QM calculated transition state. This indicated that the active site geometry of TamI L101A_L295I controls the orientation to prefer reactivity of C18 hydroxylation and therefore, is crucial in discerning the selectivity between these regioisomeric transition states.

2.4 Multifunctional TamI L295A catalyzes an unexpected and unique oxidative cascade generating tri-oxidized tirandamycin O and O' (9 and 10).

Similar to TamI L101A_L295I, TamI L295A first catalyzed *step 3* on substrate **1** producing **6**. However, divergent from the double mutant selectivity, TamI L295A catalyzes a unique series of oxidation steps leading to the formation of triple oxidation products tirandamycin O **(9)** and tirandamycin O' **(10)** (Figure 4) that eluted as a single peak during HPLC purification. In the analytical scale, a small shoulder on the major product peak is observed when incubating TamI L295A with **1** and **6**, separately, suggesting the formation of both congeners *in vitro*.

The tri-functionalized congener **9** displays an unusual oxidation pattern on the bicyclic core including a C10 keto group, a C11(*R*) hydroxyl and a C12(*S*) hydroxyl, with corresponding chemical shifts at 204 ppm, 72.1 ppm and 78.3 ppm. The relative stereochemistry of the C11(*R*) and C12(*S*) hydroxy moieties was determined by irradiation of the H-11 and H-7 protons resulted in a NOE to H-7 and H-11, respectively, while H-18 showed an NOE with H-14 and H-7, and vice versa. The ^{1}H-NMR spectrum suggests the presence of an isomer in a 5:1 mixture with **9** (C10-keto) as the predominant form. Moreover, we learned that upon storing this mixture in DMSO, the ratio of molecules changed to 3:1 with **10** (C10-hydroxy) as the major form. In **10**, the keto functionality is present at the C11 site that now displays a 205 ppm shift while the C12(*S*) hydroxyl is conserved. The C10 position harbors a hydroxy moiety in the (*S*) configuration, assigned based on the H-10 proton showing an NOE with H-17. Treatment of compound **9** (5:1) with D_2O did not show deuterium incorporation, even after extended periods of incubation (Figure S13), suggesting that protic-mediated tautomerization is not occurring. Furthermore, to elucidate the molecular basis for the exquisite stereoselectivity of the hydroxyl groups, the ΔΔG of each of the four theoretically possible stereoisomers was calculated. The experimentally observed isomer **10** was higher in energy than its C10 epimer while compound **9** was lowest in energy (Figure S14).

2.5 TamI L244A_L295V enabled a continuous 8 e^- oxidation cascade (*step 1* through *step 4)*, overriding the need for TamL

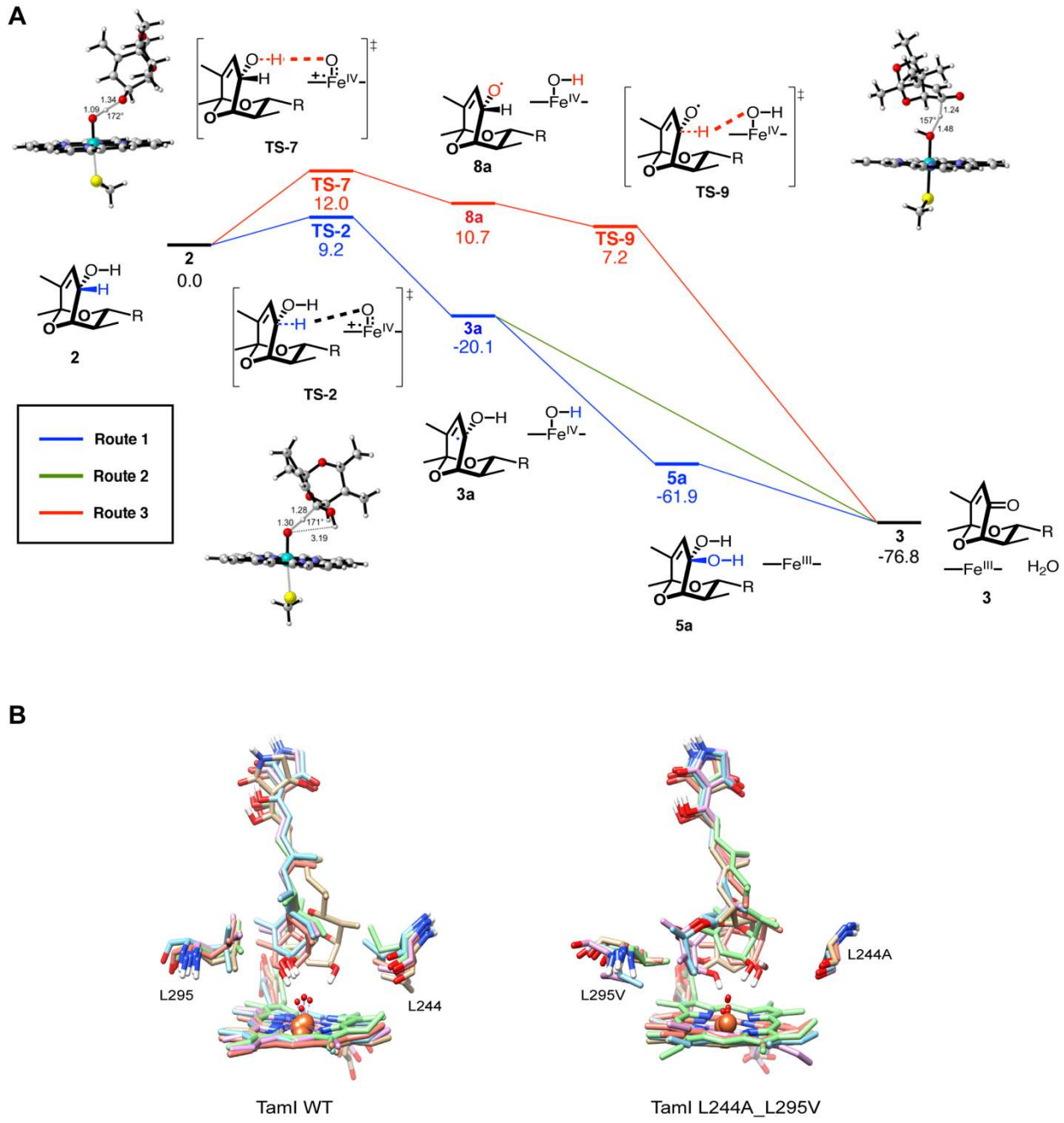

Figure 7. Computational analysis of *iterative* TamI L244A_L295V. (A) Free energy profile of potential mechanisms for the C10 ketone formation. Initial abstraction of the OH-10 proton requires a higher energetic barrier compared to H-10 abstraction, discarding Route 3 as a viable mechanism pathway. There are virtually no energetic differences that discriminate Route 1 from Route 2, suggesting that either mechanism is plausible. See also Figure S15. (B) Overlays of top five occupied clusters for **2** with TamI WT and TamI L244A_L295V.

The *iterative* TamI L244A_L295V catalyzed sequential C-H oxidation and epoxidation pathways leading to compounds **1** → **2** → **3** → **4** → **5** in a strict order as observed in the WT cascade that includes TamL (Figure 1, *step 2*).[15] However, in the absence of TamL, TamI L244A_L295V is responsible for transforming the C10(*S*) hydroxyl of **2** into a ketone, possibly

through initial formation of a geminal-diol product. To further understand this catalytic activity, we sought to explore the mechanism in which the enzyme installs the C10 keto group using DFT methods. Previous work[26, 27] provided a framework for our analysis that includes three possible mechanisms (Figure 7A). In Route 1, TamI iteratively hydroxylates at C10 forming a geminal-diol that exists predominantly in the keto form. In Route 2, the enzyme catalyzes a C10-H abstraction followed by an O-H abstraction and radical coupling to yield the ketone. Route 3 resembles Route 2 except it suggests an inverted order of proton abstraction. Analysis of the calculated free energy profiles suggests the preference of Routes 1 and 2 over Route 3 as the rate-limiting transition state is 2.8 kcal/mol higher in Route 3. In distinguishing the plausibility between Routes 1 and 2, there are virtually no energetic differences between the *gem*-diol pathway (Route 1) and the double hydrogen abstraction (Route 2), due to computation constraints that the second transition states are essentially barrierless. Thus, it is possible that either or both mechanisms are plausible with this P450 variant. Using previously described methods,[16] MD simulations of TamI L244A_L295V were performed with **2** as the substrate to assess the influence of the mutant on the selectivity within the oxidative cascade and compared with that of the TamI WT. The TamI L244A_L295V displays a higher degree of flexibility of substrate **2** with the active site compared to the WT (Figure 7B). This suggests that these mutations enable movement that is required for the C10 oxidation to occur, as our DFT mechanisms show that a shift in the binding pose is required to promote the second mechanistic steps.

4 Exploring the substrate scope, total turnover capacity and substrate binding properties of TamI biocatalysts

Effectively applying the biocatalytic potential of the engineered TamI P450s for late-stage C-H oxidation and epoxidation requires a comprehensive investigation of their substrate specificity, total turnover capacity and substrate binding affinity. We surveyed the substrate scope of TamI variants using various tirandamycin molecules and calculated the corresponding total turnover numbers (TTN) (Figure 8). Additionally, the effect of TamI mutations on the equilibrium dissociation constants (K_d) of tirandamycin substrates was assessed via substrate-induced heme spin shift experiments (Table S8).

Substrate **1**: Despite catalyzing distinct oxidation pathways, TamI WT, L295V and L101A_L295I have comparable total turnovers (TTN = 368-369) and show tight binding affinity to **1** with the double mutant displaying the strongest affinity (K_d = 0.09μM). The TamI H102V mutant that fails to generate any product when tested with **1** shows a weak binding affinity to the substrate (K_d = 10.27μM).
Substrate **2**: In addition of TamI L295V displaying epoxidase activity forming **7** from **2**, TamI WT, L295A, L101A_L295I and L244A_L295I were also found capable of catalyzing *step 3* on **2.** The double mutant L101A_L295I showed the highest TTN value of 324 and a relatively tight affinity to the substrate (K_d = 4.75μM), while no spin shift was observed with the other P450s including the parent enzyme.
Substrate **3**: Similar to WT, all variants tested with **3** catalyzed formation of the more oxidized **4** and **5**, with comparable turnover (TTN = 313-340) and binding affinities (K_d = 6.89-8.32μM). TamI

L244A_L295V and L244A_L295I led to the highest ratios of **5** to **4**, compared to TamI WT that produced the least amount of the terminal product **5**.

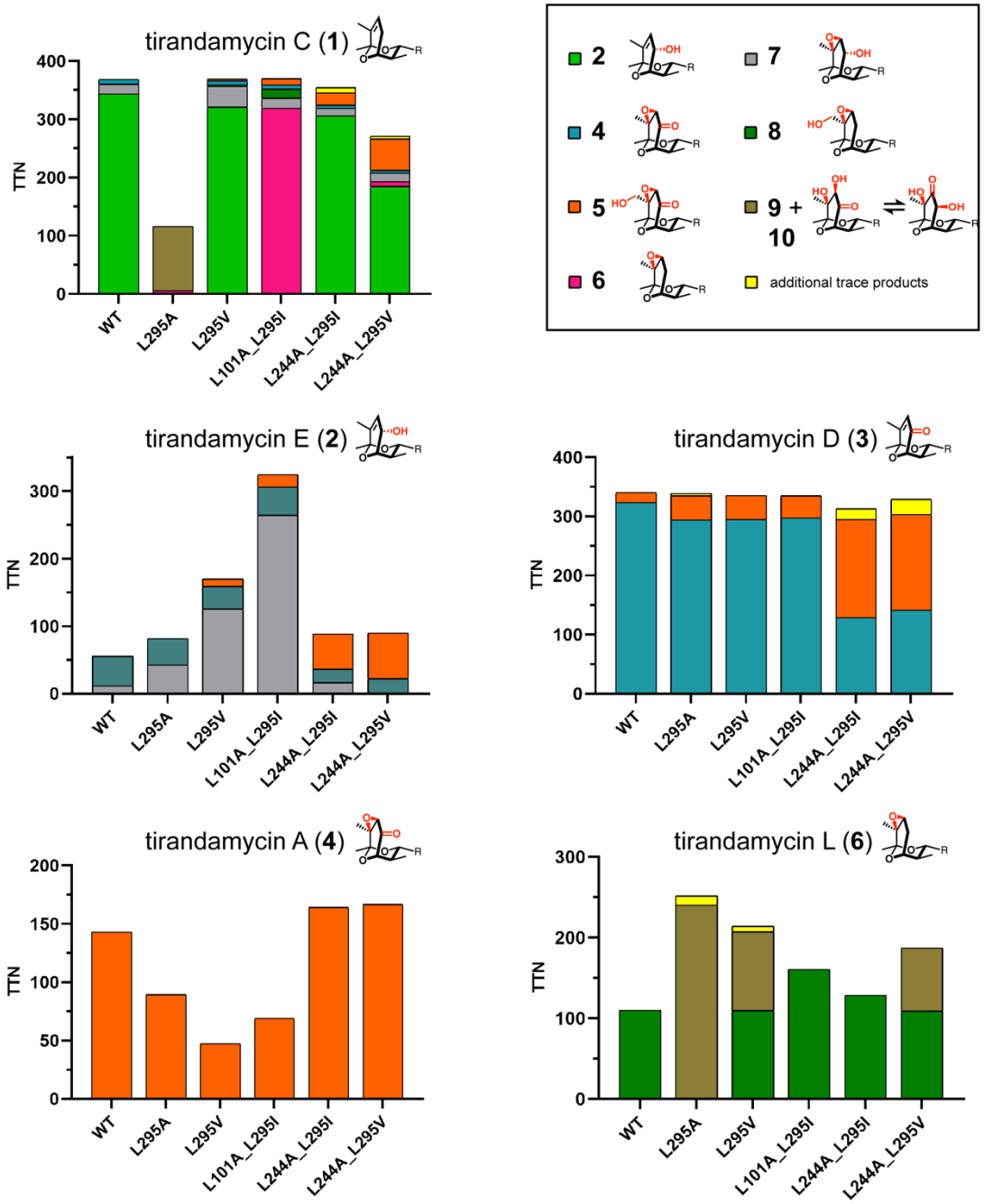

Figure 8. Total turnover numbers (TTN) for TamI WT and mutants with tirandamycins. Reaction substrates are displayed above each bar graph. TTN = mol substrate consumed/mol P450. Ratios of product formation were estimated based on HPLC data. Experiments were performed in triplicate. For exact values refer to Table S7, and for definition of R see Figure 1.

Substrate **4**: All P450s showed selectivity for *step 4,* converting **4** to **5** with *iterative* TamI P450 L244A_L295V displaying improved turnover capacity and binding affinity (TTN = 167; K_d = 7.09µM) compared to the parent enzyme (TTN = 143; K_d = no shift observed).

Substrate **6**: All P450s tested, except TamI L295A, catalyzed *step 4* on substrate **6** forming **8**. In contrast, TamI L295A generated **9** and **10** as the main products and displayed the highest TTN value of 252. No spin shift is observed when testing **6** with the P450s, except with the double mutant L101A_L295I that shows a weak binding affinity of 11.98µM.
Substrate **7**: No oxidative activity was observed when testing the substrate with TamI biocatalysts. Surprisingly, the control reaction containing TamL flavoprotein yielded complete conversion of **7** to **4** (Figure S16, lane 17). Isothermal Titration Calorimetry (ITC) was employed to measure the binding affinities of **7** and native substrate **2** with the TamL enzyme. The resulting affinities were comparable with K_d values of 1.09 and 2.26µM for **7** and **2**, respectively.
Substrates **8**, **9** and **10:** Finally, reactions with **8**, **9** and **10** failed to yield products suggesting that the engineered TamI enzymes have a limited scope for substrates with higher degrees of oxidation (Figures S17-S18).

5 Kinetic characterization of variant TamI enzymes

Michaelis-Menten kinetic parameters were determined for the various oxidation routes catalyzed by TamI WT, *selective* TamI L101A_L295I and *iterative* TamI L244A_L295V (Table 1). These enzymes were selected for testing based on their abilities to catalyze divergent iterative oxidation cascades and their enhanced binding and turnover properties.

Substrate	P450 TamI	K_M (µM)	K_{cat} (min^{-1})	K_{cat} / K_M ($\mu M^{-1} min^{-1}$)	Products observed and tracked	Step(s) catalyzed	Lane
1	WT	16.0 ± 2.6	29.8 ± 1.9	1.87	2	1	1
	L101A_L295I	3.8 ± 0.6	6.6 ± 0.3	1.71	6 + 7	3, 1	2
2	WT	108.5 ± 25.9	0.04 ± 0.01	0.0003	4 + traces of 7	2, 3	3
	L244A_L295V	115.6 ± 22.4	1.27 ± 0.10	0.0110	3 + 4 + 5 + traces of 7	2, 3, 4	4
3	WT	36.5 ± 7.1	6.8 ± 0.5	0.19	4	3	5
	L101A_L295I	120.1 ± 33.5	56.4 ± 9.6	0.4693	4	3	6
4	WT	8.2 ± 1.0	0.036 ± 0.001	0.0044	5	4	7
	L244A_L295V	7.0 ± 0.9	0.716 ± 0.023	0.1022	5	4	8
6	WT	34.9 ± 5.5	0.005 ± 0.001	0.0001	8	4	9
	L244A_L295V	55.6 ± 9.9	1.092 ± 0.066	0.0196	8 + 9 + 10	4, additional new steps	10

Table 1. Select Michaelis-Menten kinetic values. See Table S9 for additional kinetic values.

Consistent with previously described results,[15] TamI WT is most efficient at catalyzing *step 1* converting **1** to **2** with a k_{cat}/K_M value of 1.87 $\mu M^{-1}min^{-1}$ (Table 1, lane 1). Interestingly, TamI L101A_L295I catalyzes *step 3* on **1** forming **6** and the iterative oxidation of **1** to **7** (*steps 1* and *3*) with virtually the same efficiency (k_{cat}/K_M = 1.71 $\mu M^{-1}min^{-1}$) (Table 1, lane 2). As expected, TamI WT is notoriously inefficient at catalyzing the continuous oxidation of **2** to **4** (*steps 2* and *3*) (k_{cat}/K_M = 0.0003 $\mu M^{-1}min^{-1}$) (Table 1, lane 3). Compared to the WT enzyme, *iterative* TamI L244A_L295V shows a 36-fold increase of catalytic efficiency (k_{cat}/K_M = 0.011 $\mu M^{-1}min^{-1}$) when

converting **2** to **3**, **4** and **5** (*steps 2, 3* and *4*) (Table 1, lane 4). This substantial improvement in efficiency for oxidizing **2** highlights the significance of this variant in overcoming the bottleneck reaction of the cascade (*step 2*) without catalytic assistance from the TamL flavoprotein. The calculated catalytic efficiencies for *step 3* on substrate **3** forming **4** with TamI WT and TamI L101A_L295I are 0.19 and 0.47 $\mu M^{-1}min^{-1}$ (Table 1, lanes 5 and 6), while the k_{cat}/K_M value for *step 3* and *step 4* on **3** generating **4** and **5** with *iterative* TamI L244A_L295V is 0.06 $\mu M^{-1}min^{-1}$.

Moreover, the *iterative* TamI L244A_L295V is 23-times more efficient than the WT enzyme at catalyzing *step 4* on substrate **4** to generate the terminal product **5** with k_{cat}/K_M values of 0.102 and 0.004 $\mu M^{-1}min^{-1}$, respectively (Table 1, lanes 8 and 7). TamI L101A_L295I also outperforms TamI WT with a k_{cat}/K_M of 0.0375 $\mu M^{-1}min^{-1}$, suggesting an 8-fold increase in efficiency to perform the primary C-H oxidation event. Finally, TamI L101A_L295I is a more efficient catalyst than TamI WT for hydroxylation of **6** to **8** with k_{cat}/K_M values of 0.0044 and 0.0001 $\mu M^{-1}min^{-1}$ (Table 1, lane 9), respectively. *Iterative* TamI L244A_L295V shows an even higher k_{cat}/K_M value (0.0196 $\mu M^{-1}min^{-1}$) for catalyzing multiple oxidative reactions forming a mixture of **8**, **9** and **10** from substrate **6** (Table 1, lane 10).

6 Antimicrobial Testing

The naturally occurring and newly synthesized tirandamycin congeners were tested against a panel of human bacterial pathogens and their minimum inhibitory concentrations (MICs) were determined (Table 2). The activities of tirandamycins **1**, **3**, **4**, **5** and the new congener tirandamycin N (**8**) were comparable to commercial antibiotic erythromycin showing strong activity against Gram positive *B. anthracis* 34f2 and *B. cereus*. Tirandamycin B (**5**) also demonstrated enhanced activity against *S. pneumonia* ATCC 49619. Tirandamycin A (**4**) showed the strongest activity against VRE, consistent with previously described results.[19] A significant decrease in activity against VRE was observed in the new tirandamycin molecules. Poor activity was recorded for all tirandamycins against Gram negative pathogens, except for **1** that showed relatively weak activity against *E. coli* TolC.

	Ciprofloxacin	Erythromycin	Streptolydigin	5	4	1	3	2	9	8	7	6
Bacterial strain	**MIC (μM)**											
***B. anthracis* 34f2**	0.781	3.13	>100	6.25	12.5	3.13	6.25	25	>100	6.25	50	25
B. cereus	1.56	3.13	>100	3.13	6.25	3.13	25	>100	>100	50	>100	>100
Vancomycin-resistant *Enterococcus*	>100	3.13	>100	12.5	6.25	25	>100	>100	>100	>100	>100	>100
***S. pneumoniae* ATCC 49619**	1.56	0.195	>100	3.13	25	12.5	12.5	>100	>100	25	>100	>100

Table 2. Select MIC values. Tirandamycin **9** contained a minor presence of **10** in the sample in a 5:1 ratio. See Table S4 for additional MIC values.

Discussion

TamI is an iterative bacterial P450 capable of catalyzing three consecutive and highly selective oxidation reactions in a strict stepwise manner.[15] The work described herein demonstrates that this enzyme can be tuned through protein engineering to alter the selectivity, step sequence and number of reactions catalyzed, favoring either epoxidation and/or C-H activation pathways on multiple sites within a tirandamycin substrate. This tunability enabled the enzymatic synthesis of new tirandamycin derivatives with variant oxidation patterns that result from catalyst-controlled selectivity overriding innate substrate reactivity. For example, new compound **8**, which exhibits potent bioactivity against human bacterial pathogens *B. anthracis* 34f2 and *B. cereus*, is readily obtained by epoxidation and C18 methyl oxidation, whereas these oxidative decorations would normally be challenging to access in a direct fashion without competing oxidation of the existing methylene units in the substrate structure.[23-25] Our work also illustrates that TamI can be manipulated to effectively catalyze a four-step oxidative cascade without the assistance of the oxidative partner TamL, opening new avenues for the development of multifunctional oxidation catalysts with enhanced iterative properties. These results demonstrate the power of iterative bacterial P450s to develop new tools for selectivity and cascade reactions, expanding enzyme-controlled iterative C-H functionalization and epoxidation of complex scaffolds and streamlining the synthesis of high-value target compounds.

Using structure-guided mutagenesis, end-point assays and NMR analysis, active-site residues Leu101, Leu244 and Leu295 were found to be critical in dictating the selectivity features and direct oxidation cascade of TamI (Figure 4). Subtle steric alterations at the Leu295 position tuned the ability of TamI to favor either epoxidation or C-H activation pathways with exquisite control of the timing and site-selectivity of the cascade reactions from a single molecular scaffold. Specifically, starting with **1** as the substrate, TamI L295V catalyzed *step 1* followed by *step 3* yielding **7**, while TamI L295A catalyzed *step 3* generating intermediate **6** followed by successive oxidations to form tri-oxidized **9** and **10**. The TamI L101A_L295I catalyst also favored the initial epoxidation of **1** to **6** followed by *step 4* producing **8** with exquisite regioselectivity.

The ability of TamI mutants for crafting and further processing the epoxide-containing intermediate **6** yielding the more highly functionalized **8**, **9** and **10** is noteworthy. These results provide evidence that 1) *step 1* is not a prerequisite for *step 3* to occur and 2) *step 3,* as the first reaction catalyzed, does not block further oxidative reactions with TamI, catalytic limitations that are often observed with other multifunctional P450s. For example, in the mycinamicin P450 MycG,[12] an analog substrate harboring an epoxide moiety but lacking a hydroxyl cannot undergo oxidation by the catalyst due to a strict hierarchy in order of catalytic steps, where hydroxylation is imperative for subsequent epoxidation.[11] Moreover, in the iterative P450 GfsF, epoxidation is a prerequisite for hydroxylation of the 16-membered macrolactone, with no flexibility detected during the oxidative steps.[13] In both P450 MycG and P450 GfsF dual-function cascades, the step sequence seems to be fully controlled by inherent substrate reactivity and conformation. The capacity of TamI for catalyzing multi-step oxidative cascades at four distinct sites on substrate **1** (C10-C11-C12-C18) is also worth highlighting. Contrary to TamI, many iterative P450s oxidize a single site of the substrate. Examples include bacterial P450s RosC[28] and XiaM[29] that convert a

methyl group to a carboxylic acid through the corresponding alcohol and aldehyde intermediates, although more examples of P450s with similar catalytic activities are found in plants[30] and animals.[31] While same-site iterative oxidation cascades install functional groups that are critical for the bioactivity of secondary metabolites, the ability of TamI to oxidize multiple carbon atoms within a substrate enhances direct access to core structure diversification, generating new sets of analogues with different points of derivatization.

We performed computational analyses to investigate if the altered biocatalyst selectivity and chemical output observed with TamI mutants was a result of innate substrate reactivity or driven by a catalyst-controlled system. DFT calculations with **1** had previously shown that *step 3* is highest in energy compared to *step 1* and *step 4,*[16] making it the least favored reaction to occur in the absence of TamI L101A_L295I and L295A. MD simulations of the enzyme variants with **1** showed that the P450s reorient the substrate maintaining close proximity of the C11 atom to the heme center (Figure S6), thus facilitating *step 3* catalysis over *step 1*. Moreover, DFT calculations with **6** revealed that *step 1* is preferred over *step 4* (Figure 6). Once again, this contradicts the experimentally observed regioselectivity and indicates that TamI L101A_L295I overrides the innate reactivity of the substrate, achieving activation of the least electronically favored C-H bond generating **8**, a novel congener with notable bioactivity. MD simulations of TamI L101A_L295I with **6** showed that the C18 remains closer to the oxo-iron compared to C10 throughout the 1500 ns simulation, thus supporting that the enzyme environment is key in controlling regioselectivity (Figure 5B). These results illustrate that the hydrophobic interactions around the bicyclic ketal of tirandamycin, especially at the Leu295 and Leu101 sites, are most critical for redirecting oxidative pathways in TamI from an allylic C-H oxidation to an epoxidation event when starting with **1**, and for controlling the regioselectivity favoring primary over secondary hydroxylation when **6** is the substrate. It is also important to highlight that the precise control of TamI L101A_L295I for catalyzing a divergent oxidation pathway (compared to WT) does not sacrifice catalytic efficiency as the variant catalyzes *step 3* on **1** with virtually the same K_{cat}/K_M as TamI WT catalyzes *step 1* on **1** (Table 1).

Furthermore, TamI L244A_L295V was engineered to catalyze an unprecedented four-step oxidative cascade in the absence of oxidative partner TamL. The Michaelis-Menten model kinetics displayed enhanced rates of continuous oxidation of **2** (up to 36-fold) and of C18 methyl oxidation of **4** (up to 23-fold) for the TamI L244A_L295V compared to WT. These kinetic values demonstrate that by facilitating *step 2*, the TamI variant overcomes the bottleneck reaction of the pathway becoming a more efficient catalyst. Previous work with the bacterial $P450_{cam}$ demonstrated that an L244A mutation in the enzyme increased the active site malleability, enabling the oxidation of larger substrates than those accepted by the WT enzyme.[32] The authors hypothesized that the smaller alanine residue expanded the substrate-binding cavity providing a higher degree of freedom of motion for substrate positioning and catalytic function.[33] Analogous to the L244A $P450_{cam}$ system, the L244A substitution in TamI L244A_L295I generates a larger space and a higher degree of flexibility to better accommodate **2** enabling a more continuous oxidation cascade than the WT (Figure 7B). In efforts to elucidate the basis of improved iterative oxidation in TamI L244A_L295I, we propose two mechanisms for oxidation of the C10 allylic hydroxyl of **2** to a ketone either through *gem*-diol formation or double C-H abstraction (Figure

7A). Although a similar pattern of reactivity has been reported for the iterative bacterial P450 DoxA from the daunorubicin pathway,[27, 34] the free energy profile for each potential mechanism has not been previously calculated to support the mechanistic hypotheses of allylic hydroxyl oxidation in an iterative bacterial P450.

Conclusion

Investigation of TamI has provided new insights into the underlying biocatalytic mechanisms for the diverse selectivity and ordered reaction process of multifunctional P450s on complex scaffolds. Minor alterations of Leu244, Leu295 and Leu101 in the active site of TamI override substrate-controlled reactivity to enable catalyst-controlled iterative oxidation cascades, involving chemically and mechanistically distinct processes. TamI variants are able to differentiate the reactivity of the three competing sites in the unfunctionalized core structure of **1** that contains an internal 1,2-disubstituted alkene flanked by allylic methyl and allylic methylene groups. Specifically, TamI is able to selectively oxidize the C18 methyl site over the C10 methylene (observed in the production of **8**), reverse the site selectivity between an alkene and allylic C-H bond (e.g. production of **2** and **6**), and oxidize non-allylically-activated C-H bonds (as seen in the formation of **5**, and **8**-**10**, where alkene epoxidation precedes C-H oxidation). This approach enabled the enzymatic synthesis of new tirandamycins that display potent bioactivity against Gram positive human pathogens and that could be further explored for their antiparasitic activity to combat lymphatic filariasis.[20] Thus, TamI represents a compelling example for bio-inspiration given that small molecule catalysts with the potential for catalyzing both epoxidation and C-H activation are typically difficult to utilize in controlled iterative processes and present substantial challenges for catalyst-controlled site-selectivity reversals.[35-37] Additionally, our work provides a potential pathway for further protein engineering efforts with P450 homologs catalyzing multi-step oxidative cascades on a common substrate. For example, as an equivalent to TamI Leu101, dual-function P450s MycG[11] and GfsF[13] have active site non-polar residues Leu84 and Ala100, respectively, that have not yet been explored for their potential role in modulating selectivity and reaction step sequence. Similarly, equivalent to TamI Leu295, P450 GfsF contains an Ala residue at the 297 active site position, which could be modified to assess its function in controlling the native oxidation cascade and for modifying selectivity. Finally, in addition to investigating the mechanism towards formation of tri-oxidized **9** and **10**, future work will focus on substrate engineering efforts to expand the substrate scope of TamI as a versatile and highly selective P450 biocatalyst for iterative late-stage C-H oxidation and epoxidation of complex bicyclic and polycyclic scaffolds.

Author information

Corresponding authors
*davidhs@umich.edu

ORCID
David H. Sherman: 0000-0001-8334-3647
John Montgomery: 0000-0002-2229-0585
K. N. Houk: 0000-0002-8387-5261

Rosa V. Espinoza: 0000-0003-0007-7959

Notes
The authors declare no competing financial interest.

Acknowledgments
The authors thank the National Science Foundation under the CCI Center for Selective C−H Functionalization (CHE-1700982), the National Institutes of Health (R35 GM118101 and R35GM118133), and the Hans W. Vahlteich Professorship (to D.H.S.) for financial support.

References

1. Meunier, B.; de Visser, S. P.; Shaik, S. Mechanism of oxidation reactions catalyzed by cytochrome p450 enzymes. *Chem Rev* **2004,** 104, 3947-80.
2. Ortiz de Montellano, P. R. Hydrocarbon hydroxylation by cytochrome P450 enzymes. *Chem Rev* **2010,** 110, 932-48.
3. Lowell, A. N.; DeMars, M. D., 2nd; Slocum, S. T.; Yu, F.; Anand, K.; Chemler, J. A.; Korakavi, N.; Priessnitz, J. K.; Park, S. R.; Koch, A. A.; Schultz, P. J.; Sherman, D. H. Chemoenzymatic Total Synthesis and Structural Diversification of Tylactone-Based Macrolide Antibiotics through Late-Stage Polyketide Assembly, Tailoring, and C-H Functionalization. *J Am Chem Soc* **2017,** 139, 7913-7920.
4. Fessner, N. D. P450 Monooxygenases Enable Rapid Late-Stage Diversification of Natural Products via C-H Bond Activation. *ChemCatChem* **2019,** 11, 2226-2242.
5. Cochrane, R. V.; Vederas, J. C. Highly selective but multifunctional oxygenases in secondary metabolism. *Acc Chem Res* **2014,** 47, 3148-61.
6. Mizutani, M.; Sato, F. Unusual P450 reactions in plant secondary metabolism. *Arch Biochem Biophys* **2011,** 507, 194-203.
7. Espinoza, R. V.; Sherman, D. H. Exploring the molecular basis for selective C-H functionalization in plant P450s. *Synth Syst Biotechnol* **2020,** 5, 97-98.
8. Hang, L.; Liu, N.; Tang, Y. Coordinated and Iterative Enzyme Catalysis in Fungal Polyketide Biosynthesis. *ACS Catal* **2016,** 6, 5935-5945.
9. Podust, L. M.; Sherman, D. H. Diversity of P450 enzymes in the biosynthesis of natural products. *Nat Prod Rep* **2012,** 29, 1251-66.
10. Roiban, G. D.; Agudo, R.; Reetz, M. T. Cytochrome P450 catalyzed oxidative hydroxylation of achiral organic compounds with simultaneous creation of two chirality centers in a single C-H activation step. *Angew Chem Int Ed Engl* **2014,** 53, 8659-63.
11. Yang, S.; DeMars, M. D., 2nd; Grandner, J. M.; Olson, N. M.; Anzai, Y.; Sherman, D. H.; Houk, K. N. Computational-Based Mechanistic Study and Engineering of Cytochrome P450 MycG for Selective Oxidation of 16-Membered Macrolide Antibiotics. *J Am Chem Soc* **2020,** 142, 17981-17988.
12. Anzai, Y.; Li, S.; Chaulagain, M. R.; Kinoshita, K.; Kato, F.; Montgomery, J.; Sherman, D. H. Functional analysis of MycCI and MycG, cytochrome P450 enzymes involved in biosynthesis of mycinamicin macrolide antibiotics. *Chem Biol* **2008,** 15, 950-9.

13. Miyanaga, A.; Takayanagi, R.; Furuya, T.; Kawamata, A.; Itagaki, T.; Iwabuchi, Y.; Kanoh, N.; Kudo, F.; Eguchi, T. Substrate Recognition by a Dual-Function P450 Monooxygenase GfsF Involved in FD-891 Biosynthesis. *Chembiochem* **2017,** 18, 2179-2187.
14. Richter, M. E.; Traitcheva, N.; Knupfer, U.; Hertweck, C. Sequential asymmetric polyketide heterocyclization catalyzed by a single cytochrome P450 monooxygenase (AurH). *Angew Chem Int Ed Engl* **2008,** 47, 8872-5.
15. Carlson, J. C.; Li, S.; Gunatilleke, S. S.; Anzai, Y.; Burr, D. A.; Podust, L. M.; Sherman, D. H. Tirandamycin biosynthesis is mediated by co-dependent oxidative enzymes. *Nat Chem* **2011,** 3, 628-633.
16. Newmister, S. A.; Srivastava, K. R.; Espinoza, R. V.; Caddell Haatveit, K.; Khatri, Y.; Martini, R. M.; Garcia-Borràs, M.; Podust, L. M.; Houk, K. N.; Sherman, D. H. Molecular Basis of Iterative C–H Oxidation by TamI, a Multifunctional P450 Monooxygenase from the Tirandamycin Biosynthetic Pathway. *ACS Catalysis* **2020,** 10, 13445-13454.
17. Carlson, J. C.; Fortman, J. L.; Anzai, Y.; Li, S.; Burr, D. A.; Sherman, D. H. Identification of the tirandamycin biosynthetic gene cluster from Streptomyces sp. 307-9. *Chembiochem* **2010,** 11, 564-72.
18. Meyer, C. E. Tirandamycin, a new antibiotic isolation and characterization. *J Antibiot (Tokyo)* **1971,** 24, 558-60.
19. Carlson, J. C.; Li, S.; Burr, D. A.; Sherman, D. H. Isolation and characterization of tirandamycins from a marine-derived Streptomyces sp. *J Nat Prod* **2009,** 72, 2076-9.
20. Yu, Z.; Vodanovic-Jankovic, S.; Ledeboer, N.; Huang, S. X.; Rajski, S. R.; Kron, M.; Shen, B. Tirandamycins from Streptomyces sp. 17944 inhibiting the parasite Brugia malayi asparagine tRNA synthetase. *Org Lett* **2011,** 13, 2034-7.
21. Ogasawara, Y.; Kondo, K.; Ikeda, A.; Harada, R.; Dairi, T. Identification of tirandamycins as specific inhibitors of the futalosine pathway. *J Antibiot (Tokyo)* **2017,** 70, 798-800.
22. Yeom, E.; Kwon, D. W.; Lee, J.; Kim, S. H.; Lee, J. H.; Min, K. J.; Lee, K. S.; Yu, K. Asparaginyl-tRNA Synthetase, a Novel Component of Hippo Signaling, Binds to Salvador and Enhances Yorkie-Mediated Tumorigenesis. *Front Cell Dev Biol* **2020,** 8, 32.
23. Yoshimura, H.; Takahashi, K.; Ishihara, J.; Hatakeyama, S. Unified synthesis of tirandamycins and streptolydigins. *Chem Commun (Camb)* **2015,** 51, 17004-7.
24. Takahashi, K.; Harada, R.; Hoshino, Y.; Kusakabe, T.; Hatakeyama, S.; Kato, K. Formal synthesis of tirandamycin B. *Tetrahedron* **2017,** 73, 3548-3553.
25. Yadav, J. S.; Dhara, S.; Mohapatra, D. K. Stereoselective total synthesis of 10-epi-tirandamycin E. *Tetrahedron* **2017,** 73, 1358-1366.
26. Grandner, J. M.; Cacho, R. A.; Tang, Y.; Houk, K. N. Mechanism of the P450-Catalyzed Oxidative Cyclization in the Biosynthesis of Griseofulvin. *ACS Catal* **2016,** 6, 4506-4511.
27. Bellucci, G.; Chiappe, C.; Pucci, L.; Gervasi, P. G. The mechanism of oxidation of allylic alcohols to alpha,beta-unsaturated ketones by cytochrome P450. *Chem Res Toxicol* **1996,** 9, 871-4.
28. Iizaka, Y.; Takeda, R.; Senzaki, Y.; Fukumoto, A.; Anzai, Y. Cytochrome P450 enzyme RosC catalyzes a multistep oxidation reaction to form the non-active compound 20-carboxyrosamicin. *FEMS Microbiol Lett* **2017,** 364.

29. Zhang, Q.; Li, H.; Li, S.; Zhu, Y.; Zhang, G.; Zhang, H.; Zhang, W.; Shi, R.; Zhang, C. Carboxyl formation from methyl via triple hydroxylations by XiaM in xiamycin A biosynthesis. *Org Lett* **2012,** 14, 6142-5.
30. Ro, D. K.; Paradise, E. M.; Ouellet, M.; Fisher, K. J.; Newman, K. L.; Ndungu, J. M.; Ho, K. A.; Eachus, R. A.; Ham, T. S.; Kirby, J.; Chang, M. C.; Withers, S. T.; Shiba, Y.; Sarpong, R.; Keasling, J. D. Production of the antimalarial drug precursor artemisinic acid in engineered yeast. *Nature* **2006,** 440, 940-3.
31. Pikuleva, I. A.; Bjorkhem, I.; Waterman, M. R. Expression, purification, and enzymatic properties of recombinant human cytochrome P450c27 (CYP27). *Arch Biochem Biophys* **1997,** 343, 123-30.
32. Verras, A.; Alian, A.; de Montellano, P. R. Cytochrome P450 active site plasticity: attenuation of imidazole binding in cytochrome P450(cam) by an L244A mutation. *Protein Eng Des Sel* **2006,** 19, 491-6.
33. Voss, J. J. D.; Sibbesen, O.; Zhang, Z.; Montellano, P. R. O. d. Substrate Docking Algorithms and Prediction of the Substrate Specificity of Cytochrome P450cam and Its L244A Mutant. *J. Am. Chem. Soc.* **1997,** 119, 5489-5498.
34. Dickens, M. L.; Priestley, N. D.; Strohl, W. R. In vivo and in vitro bioconversion of epsilon-rhodomycinone glycoside to doxorubicin: functions of DauP, DauK, and DoxA. *J Bacteriol* **1997,** 179, 2641-50.
35. Newhouse, T.; Baran, P. S. If C-H bonds could talk: selective C-H bond oxidation. *Angew Chem Int Ed Engl* **2011,** 50, 3362-74.
36. White, M. C. Chemistry. Adding aliphatic C-H bond oxidations to synthesis. *Science* **2012,** 335, 807-9.
37. Neufeldt, S. R.; Sanford, M. S. Controlling site selectivity in palladium-catalyzed C-H bond functionalization. *Acc Chem Res* **2012,** 45, 936-46.